Sulfur Cathodes with Hydrogen Reduced Titanium Dioxide Inverse Opal Structure

Zheng Liang,[†,⊥] Guangyuan Zheng,[‡,⊥] Weiyang Li,[†] Zhi Wei Seh,[†] Hongbin Yao,[†] Kai Yan,[†] Desheng Kong,[†] and Yi Cui[†,§,*]

[†]Department of Materials Science and Engineering and [‡]Department of Chemical Engineering, Stanford University, Stanford, California 94305, United States, and [§]Stanford Institute for Materials and Energy Sciences, SLAC National Accelerator Laboratory, 2575 Sand Hill Road, Menlo Park, California 94025, United States. [⊥]Zheng Liang and Guangyuan Zheng contributed equally to this work.

ABSTRACT Sulfur is a cathode material for lithium-ion batteries with a high specific capacity of 1675 mAh/g. The rapid capacity fading, however, presents a significant challenge for the practical application of sulfur cathodes. Two major approaches that have been developed to improve the sulfur cathode performance include (a) fabricating nanostructured conductive matrix to physically encapsulate sulfur and (b) engineering chemical modification to enhance binding with polysulfides and, thus, to reduce their dissolution. Here, we report a three-dimensional (3D) electrode structure to achieve both sulfur physical encapsulation and polysulfides binding simultaneously. The electrode is based on hydrogen reduced TiO_2 with an inverse opal structure that is highly conductive and robust toward electrochemical cycling. The relatively enclosed 3D structure provides an ideal architecture for sulfur and polysulfides confinement. The openings at the top surface allow sulfur infusion into the inverse opal structure. In addition, chemical tuning of the TiO_2 composition through hydrogen reduction was shown to enhance the specific capacity and cyclability of the cathode. With such TiO_2 encapsulated sulfur structure, the sulfur cathode could deliver a high specific capacity of ~1100 mAh/g in the beginning, with a reversible capacity of ~890 mAh/g after 200 cycles of charge/discharge at a *C*/5 rate. The Coulombic efficiency was also maintained at around 99.5% during cycling. The results showed that inverse opal structure of hydrogen reduced TiO_2 represents an effective strategy in improving lithium sulfur batteries performance.

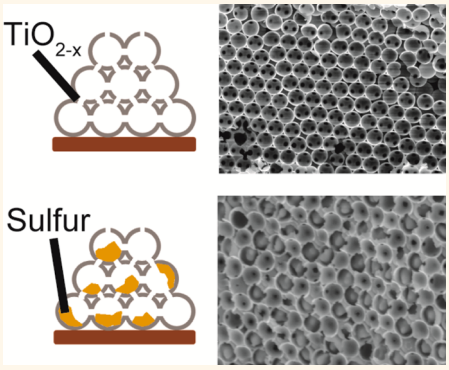

KEYWORDS: lithium sulfur battery · sulfur cathodes · hydrogen reduced TiO_2 · TiO_2 inverse opal · high electrochemical performance

Because of the environmental issue caused by fossil fuel and recent emerging consumer desire for portable electronic devices, there is a strong demand for high performance energy storage technologies.[1] Secondary lithium-ion batteries (LIB) have successfully drawn great attention due to their high energy density, high power density, as well as their long cycle life.[2] Research into anode materials in secondary LIB has seen tremendous progress with the successful demonstration of high specific capacity in silicon nanostructures.[3−7] Whereas the specific capacity of silicon can reach around 3000 mAh/g (with theoretical value of 4200 mAh/g), the practical specific capacity for most commercial transition metal oxide cathodes is limited to 200 mAh/g.[8,9] The mismatch in the cathode/anode pairs and the relatively slow research progress on cathodes become a big hurdle in fully exploiting the potential of lithium-ion batteries.

Sulfur has been widely studied as a high-energy-density cathode material to replace the traditional metal oxides.[10] When pairing with Li metal anodes, sulfur system can deliver a specific capacity as high as 1675 mAh/g and an energy density of 2500 Wh/kg or 2800 Wh/L. Moreover, the natural abundance and low cost of sulfur further make this material attractive as advanced cathode materials.[11,12] Despite the various advantages, sulfur cathodes suffer from several inherent challenges. Sulfur itself and the discharge product lithium sulfide are both insulating (conductivity of elemental sulfur can be as low as 5×10^{-30} S/cm at room temperature),[13] which leads to the limited utilization of active material and low rate

* Address correspondence to yicui@stanford.edu.

Received for review March 6, 2014 and accepted April 26, 2014.

Published online April 26, 2014
10.1021/nn501308m

capability along with a poor electrochemical reversibility. Sulfur cathodes face a significant volume change (up to 80%) during discharge.[14,15] Moreover, the lithium polysulfides (Li_2S_n, $4 < n < 8$) formed as intermediate products during the charge/discharge process are highly soluble in the organic electrolyte.[11,16−18] Dissolved lithium polysulfides diffuse to the lithium anode and then get reduced into lower order polysulfides. These lower order polysulfides can diffuse back to the cathode during cycling to cause the "shuttle effect",[19] which gives rise to the fast capacity decay, low Coulombic efficiency and limited cycle performance.[19]

Various strategies have been explored to address the aforementioned issues. An ideal sulfur immobilizer should be a conductive (ionically and electrically) framework with the ability to effectively trap polysulfides. Carbon-based hosts, such as carbon nanotubes,[20] mesoporous carbon,[9] carbon fiber,[21] and graphene,[22] have been extensively studied for sulfur cathodes. These sulfur/carbon composites have been shown to have good physical confinement of sulfur as well as polysulfides. Another rational design consists of hindering polysulfides dissolution by chemical adsorption through the employment of conductive polymer[23−25] or metal oxide additives including TiO_2,[26] Al_2O_3,[27] La_2O_3,[28] $Mg_{0.8}Cu_{0.2}O$,[29] and $Mg_{0.6}Ni_{0.4}O$.[30]

However, complexity involved in design and manufacturing process reduces the feasibility. To develop a solution that solves the sulfur cathode issues simultaneously, one potential approach is to integrate all these designs.

Herein, we combine all the design criteria into a simple integrated electrode structure, to minimize the complexity in the synthesis of several key attributes into one system. We report the application of hydrogen reduced TiO_2 inverse opal as a favorable candidate for sulfur cathodes with the following attributes: (1) Hydrogen treated TiO_2 gains a dramatic increase in conductivity making this large bandgap semiconductor a promising current collector. (2) Rapid electron and lithium-ion transport is facilitated by the 3D framework and thin TiO_2 shell (~25 nm). (3) The oxygen vacancies generated during reduction process may promote the interaction between TiO_2 and sulfur (S−Ti−O), which can improve the TiO_2 surface adsorption of polysulfides.[31] (4) Our design has successfully achieved the integration of physical confinement and chemical adsorption of polysulfides.

RESULTS AND DISCUSSION

As schematically summarized in Figure 1, the inverse opal structure was prepared using a polystyrene opal template method. Polystyrene colloidal spheres are versatile materials for fabricating nanomaterials and 3D frameworks in energy applications,[32,33] owing to its low cost and self-assembly nature.[34,35] The polystyrene

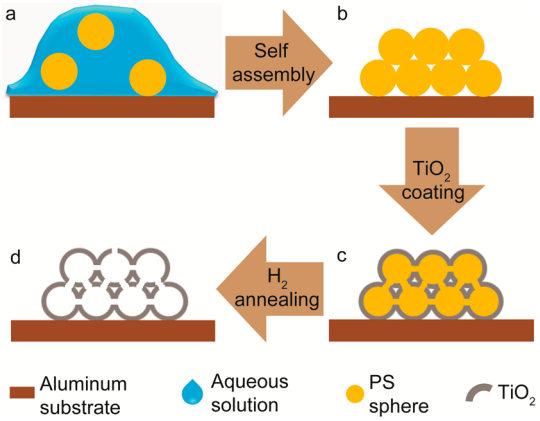

Figure 1. Schematics of the fabrication processes of hydrogen reduced TiO_2 inverse opal: (a) polystyrene spheres (yellow) dispersed in aqueous suspension; (b) polystyrene spheres self-assembly into hexagonally close-packed structure in the drying process; (c) amorphous TiO_2 deposited through low temperature ALD; (d) polystyrene template removed in hydrogen annealing.

nanoparticles aqueous suspension was drop-casted onto an aluminum substrate (Figure 1a). In the drying process, the polystyrene spheres self-assemble to form a close-packed layer-by-layer network (Figure 1b). The 3D ordered structure served as a template for TiO_2 growth. Amorphous TiO_2 was formed on the polystyrene spheres through a low temperature atomic layer deposition (ALD) with oxygen plasma pretreatment to ensure conformal coating (Figure 1c). The polystyrene template was removed after annealing in hydrogen atmosphere (Figure 1d).

Figure 2 demonstrated the morphology of the as-prepared inverse opal. It reveals a 3D hierarchically porous framework consisting of highly ordered nanopores (780 nm in diameter) interconnected with each other by channels (Figure 2a). These open channels were formed due to the contact area between neighboring polystyrene colloidal spheres. The thickness of the layer is uniform at around 15 μm depending on the amount of the latex suspension added (Figure S1, Supporting Information). Figure 2b,c shows the digital camera images of the sample before (b)and after (c) polystyrene template removal. Titania after hydrogen reduction treatment presents a darker color, suggesting the presence of metallic Ti^{3+} ions.[36,37] The nanoscale hollow structure offers enough space for discharge products deposition and sulfur volume expansion during cycling. Moreover, the 3D interconnected network along with open channels allows facile electrolyte permeation and fast ionic transport. In addition, the complex architecture and TiO_2 itself effectively retain polysulfides both by physical trapping and chemical interaction. These attributes of this structure enable high specific capacity and remarkable cycle stability in the Li−S system. The typical transmission electron microscopy (TEM) images of this structure are shown in Figure 2d,e indicating the planar

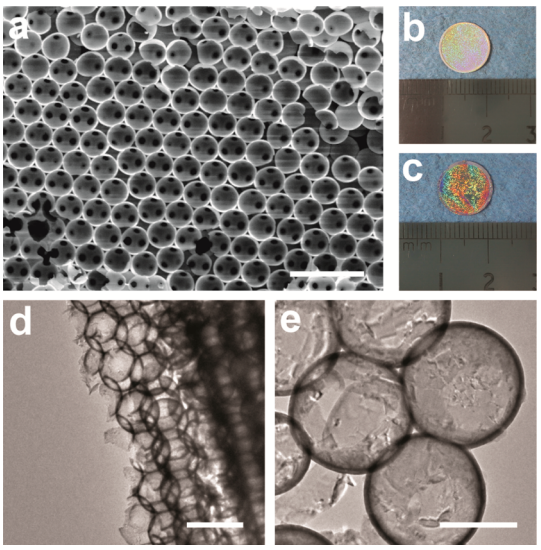

Figure 2. Morphology of the reduced TiO_2 inverse opal: (a) cross-sectional SEM image of the 3D ordered reduced TiO_2 structure; (b and c) digital camera images of the as-prepared TiO_2 inverse opal before (b) and after (c) hydrogen annealing; (d and e) TEM images (d) of the reduced hollow TiO_2 nanosphere structure and (e) zoom-in of the reduced TiO_2 nanosphere. The thickness of the nanosphere wall is around 25 nm. Scale bars in (a), (d), and (e) are 2, 1 and 0.5 μm, respectively.

hexagonal arrangement. The shell thickness is about 25 nm.

It has been reported that electrical conductivity of TiO_2 can be substantially enhanced with the presence of oxygen vacancies and Ti^{3+} species.[38] Therefore, annealing TiO_2 in a reducing gas atmosphere effectively increases the oxygen vacancy density and thereby modifies the electronic properties.[39,40]

After annealed in hydrogen, the oxygen deficient titania (TiO_{2-x}) was characterized by XRD (Figure 3c). The diffraction pattern reveals multiple phases existing in the product. The identified peaks are indexed as anatase TiO_2 (JCPDS card No. 89-4203), rutile TiO_2 (JCPDS card No. 79-5860) and brookite TiO_2 (JCPDS card No. 76-1937), although the latter two exist in relatively smaller portions. Hydrogen annealing would facilitate the phase transformation from anatase to rutile at a lower temperature.[41] Brookite in the mixture was the intermediate product.

To further probe the electronic and chemical environment, X-ray photoelectron spectroscopy (XPS) analysis was performed. The binding energies were calibrated with respect to the C 1s peak at 284.5 eV. Figure 3a illustrates the Ti 2p core level spectra for control TiO_2 (unreduced) and hydrogen reduced TiO_2. Both spectra were normalized to the same intensity for clear comparison. The control TiO_2 sample shows two predominant peaks at 464.6 and 458.7 eV, which are attributed to the characteristic Ti $2p_{1/2}$ and Ti $2p_{3/2}$ peaks of Ti^{4+}.[39,42] For reduced TiO_2, it clearly exhibits a red shift in binding energy, indicating the different chemical environment for titanium cations in the

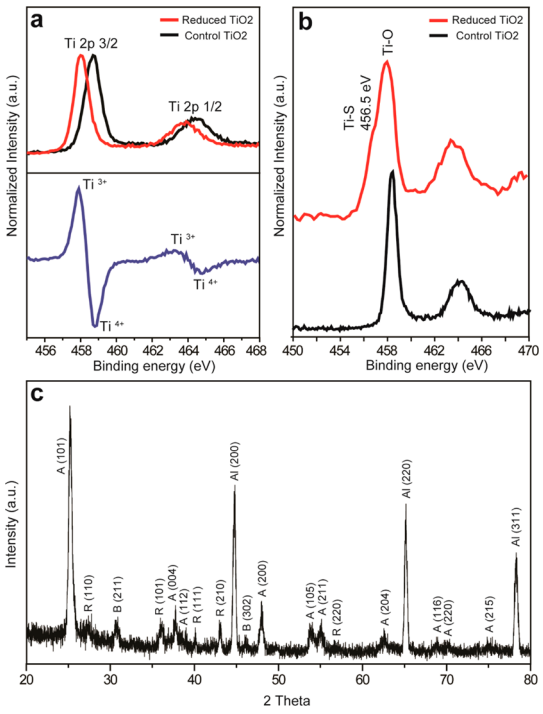

Figure 3. XPS and XRD characterizations. (a) Top part is the normalized Ti 2p XPS spectra of reduced TiO_2 (red solid curve) and control TiO_2 (black solid curve); bottom part is their subtraction spectrum. (b) Normalized Ti 2p XPS spectra of polysulfides treated TiO_2. Red solid curve is reduced TiO_2 after polysulfides treatment; black solid curve is control TiO_2 after polysulfides treatment. (c) XRD pattern collected from the reduced TiO_2 (A, anatase; R, rutile; B, brookite; Al, aluminum substrate).

hydrogenated phase. Two extra peaks exist at 463.2 and 457.9 eV by subtracting the Ti 2p spectra of reduced TiO_2 with control TiO_2. These two peaks are within the range of published Ti^{3+} 2p binding energies.[39,43,44] It further confirms the presence of Ti^{3+} cations created in the hydrogenation process. The less positively charged Ti^{3+} nuclei leads to an increment in electron density and therefore a weaker binding effect.[39]

Interaction between reduced TiO_2 and polysulfides was also examined by mixing them together under vigorous stirring for 5 days. The polysulfides treated TiO_2 was then dried in argon atmosphere before XPS characterization. Compared to the control TiO_2 sample, the Ti $2p_{3/2}$ XPS peak of polysulfides treated TiO_{2-x} was found to be broader, as shown in Figure 3b top. An additional shoulder appeared around 456.5 eV for the treated hydrogen reduced TiO_2, which lies in the range of published Ti−S binding energies (~456.4 eV).[45−47] It thus suggests the presence of Ti−S interaction. One of the possible mechanisms of Ti−S interaction in bulk TiO_2 is the chemical adsorption of sulfur in intrinsic oxygen vacancies.[43] Hydrogen annealing substantially promotes the formation of oxygen vacancies and therefore facilitates the interaction between TiO_2 and polysulfides when applied to sulfur cathodes.

The TiO_{2-x}/sulfur composite material was fabricated by a simple melt-diffusion process. The mixture was held for 12 h at elevated temperate to allow sulfur infiltration from free openings at the top surface (Figure S2, Supporting Information) into the porous structure under capillary forces. Subsequently, as-prepared sulfur impregnated sample was treated with methanol to remove excessive sulfur. Figure S3 (Supporting Information) is the top view of the TiO_{2-x} morphology after sulfur impregnation and methanol treatment. Little sulfur is deposited on the top surface. On the basis of the evidence together with the cross section view (Figure 4a) and energy-dispersive X-ray spectroscopy (EDS) mappings (Figure 4b to 4d), we conclude that sulfur is mainly homogeneously coated onto the inner surface instead of the exterior surface. Intensive research has been conducted on porous texture carbon based matrix sulfur composites. However, there are still large amounts of sulfur residue outside the matrix. As a result, sulfur was directly in contact with electrolyte without any trapping.[20,48] So the polysulfides dissolution issue remains unsolved. In the present study, we attempt to tackle this issue to achieve excellent cycle stability.

To test the electrochemical performance of the integrated TiO_{2-x}/sulfur nanocomposite, coin cells were assembled with lithium foil as counter/reference electrode along with TiO_{2-x}/sulfur nanocomposite as the working electrode without any binder or conductive additives. The typical S mass loading was 0.8 mg/cm^2 and the battery capacities were all calculated based on sulfur mass, which was determined by measuring the mass difference of the electrode before and after sulfur infusion. The cells were cycled from 1.8 to 2.6 V *versus* Li^+/Li.

Figure 5a depicts the typical cyclic voltammetry (CV) curves at a constant scan rate of 0.2 mV/s in the voltage range of 1.0−3.0 V. Two pronounced cathodic peaks at approximately 2.26 and 1.92 V are observed. The peak at 2.26 V corresponds to the transition from elemental sulfur to long chain lithium polysulfides (Li_2S_n, $4 < n < 8$). The peak at 1.92 V is related to the further reduction of low order lithium polysulfides to Li_2S_2 and Li_2S. A broader anodic peak is observed in the potential around 2.75 V with a shoulder at 2.8 V, which is attributed to the reverse reactions in the charging stage. The subsequent peaks located at 1.7 V

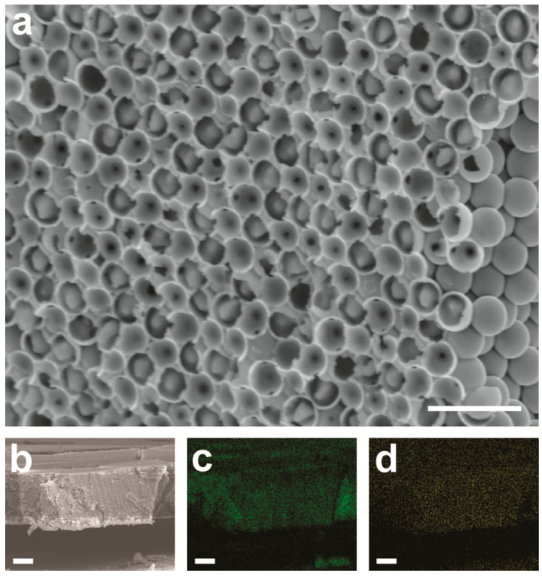

Figure 4. SEM and EDS characterization of the reduced TiO_2 inverse opal structure after sulfur infusion; (a) cross-sectional SEM image of the composite structure showing sulfur particles well encapsulated by the reduced TiO_2 nanospheres; (b−d) SEM image of the electrode cross section (b) and the corresponding elemental mapping for sulfur (c) and titanium (d). Scale bars are 2 μm in (a), and 5 μm in (b−d).

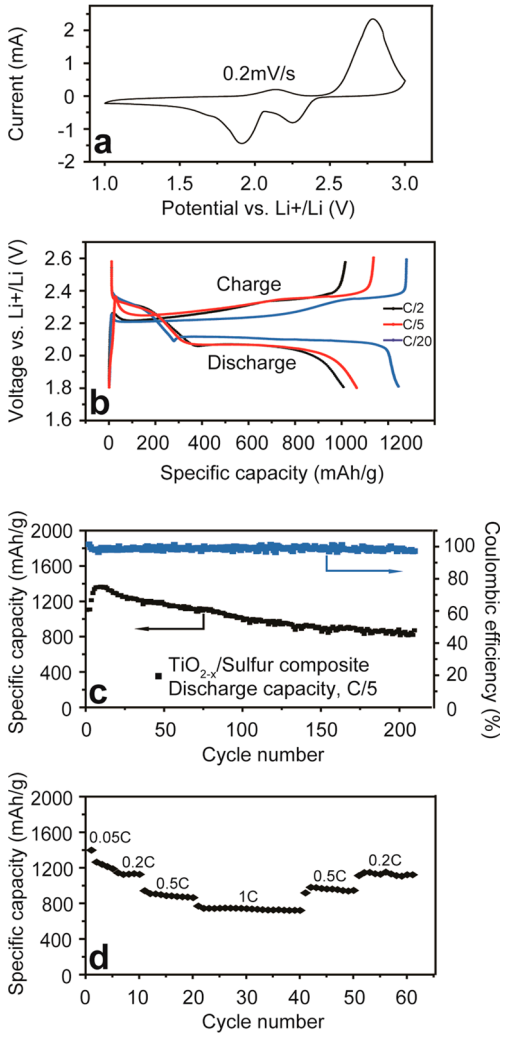

Figure 5. Electrochemical testing and battery performance of the reduced TiO_2 inverse opal-encapsulated sulfur cathodes: (a) cyclic voltammetry of the TiO_{2-x}/sulfur cathode obtained at 0.2 mV/s; (b) typical charge/discharge profiles at different current rates (1*C* = 1675 mAh/g); (c) cycling performance (black curve) and Coulombic efficiency (blue curve) of TiO_{2-x}/sulfur composite cathode at a current rate of *C*/5; (d) rate performance of the composite cathode at different *C* rates ranging from 0.05C to 1C.

(shoulder peak) and 2.15 V reveal the lithiation and delithiation of anatase TiO_2 which is generally in agreement with previous research results.[49,50] Although there is concern that lithium may intercalate into rutile/brookite TiO_2 which would affect the electrical conductivity, based on the CV curve, lithiation of rutile/brookite TiO_2 was not observed within the voltage range that have been specified by literatures.[51,52] To conclude, the CV results indicate that reduced titania functions as a decent electrical conductor in good contact with sulfur encapsulated inside.

For further study of the electrochemical properties, charge/discharge voltage profiles are shown in Figure 5b as a function of specific capacity at different current rates (*C*/20, *C*/2, *C*/5, where 1*C* = 1675 mA/g). Consistent with CV curves, these discharge voltage profiles display the typical two-plateau behavior of Li−S system, corresponding to the formation of high order polysulfides (Li_2S_n, $4 < n < 8$) at 2.3 V and Li_2S_2 and Li_2S at 2.1 V. Moreover, the flat second discharge plateau indicates a small kinetic barrier. The discharge voltage cutoff is set at 1.8 V to eliminate capacity contributed from TiO_2 lithiation. At a low current rate of *C*/20, a high specific capacity of 1250 mAh/g is obtained without any noticeable overpotential. As current rate increases, the specific capacity is reduced slightly to 1050 mAh/g at *C*/5 and 990 mAh/g at *C*/2. The limited capacity drop at various rates associates with the good kinetics of the structure. In addition, no plateau from reaction of lithium with TiO_2 was observed by setting the discharge voltage cutoff at 1.8 V.

The long-term cycling stability is a critical issue for practical application. Here, the TiO_{2-x}/sulfur electrode was cycled at the *C*/5 rate (Figure 5c). The discharge capacity starts at 1100 mAh/g and displays a gradual increase for first eight cycles. It suggests an activation step during the first several cycles, mainly due to electrolyte diffusion through the complex structure. The TiO_{2-x}/sulfur electrode exhibits a reversible capacity of 890 mAh/g after 200 cycles, corresponding to capacity retention of 81% over 200 cycles. The average Coulombic efficiency is around 99.5%. These results show improved performance compared to previous studies in our group on carbon nanofiber encapsulated sulfur cathodes,[21] graphene-wrapped sulfur structures,[22] and biotemplate assisted nanostructured sulfur batteries.[53] In addition, Figure S4 shows the comparison of cycling performances of our sample and the control sample without hydrogen reduction. The hydrogen reduced TiO_2 encapsulated sulfur cathode demonstrates enhanced discharge capacity and cycling stability compared to the unreduced sample. The good capacity retention for the reduced TiO_2 sample is due to the significant role of reduced TiO_2 that combines the physical entrapment from hierarchical porous structure along with chemical bonding between TiO_2 and polysulfides. Current−voltage measurement was also performed on the reduced TiO_2 as well as control TiO_2 to confirm the electrical conductivity improvement (Figure S5). Rate performances from *C*/20 to 1*C* are presented in Figure 5d. The battery delivers a reversible discharge capacity of 1400, 1150, 900, and 780 mAh/g at *C*/20, *C*/5, *C*/2 and 1*C*, respectively. The good rate capability is related to good electrical conductivity of reduced TiO_2 and 3D access of liquid electrolyte. The capacity almost returns to the original capacity at *C*/5 when the rate is readjusted to *C*/5. The steadily change of the discharge capacities over different current rates indicates robustness and stability of the cathode structure. Moreover, the good rate capability reveals facile ion/electron transport as well as electrolyte accessibility.

The stability of Ti^{3+} species toward electrochemical cycling is also crucial. The TiO_{2-x} conductive matrix would lose its electrical conductivity resulting in the deterioration of the electrochemical performance if Ti^{3+} is reoxidized to Ti^{4+} during the charging process. The standard reduction potential of Ti^{4+}/Ti^{3+} is 2.5 V *versus* Li^+/Li which is close to our charge voltage cutoff.[54] Taking the overpotential during our battery operation into consideration, the reoxidation of Ti^{3+} is beyond the scope. Moreover, no anodic peaks associated with Ti^{4+}/Ti^{3+} transition were observed according to CV curve.

Little change in morphology was observed before and after lithiation. SEM image of the TiO_{2-x}/sulfur nanocomposite electrode after 100th cycle shows a structurally intact TiO_2 coating (Figure 6), confirming the structure is able to tolerate sulfur volume expansion during the lithiation process. The preservation of the 3D inverse opal network during battery operations indicates the robustness of the electrode. We understand the structure stability of TiO_{2-x} framework according to the following three reasons: (1) the empty space designed inside the TiO_{2-x} inverse opal can

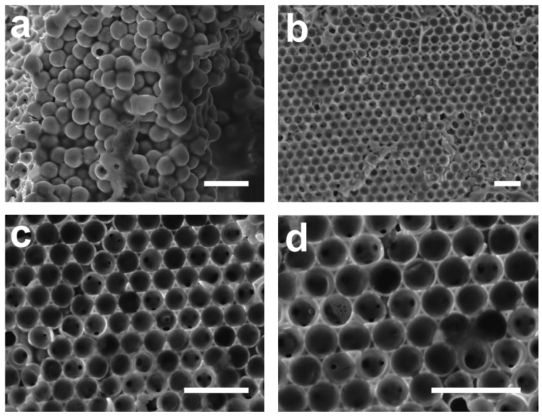

Figure 6. Structural characterization of TiO_{2-x}/sulfur composite cathode after the 100th discharge. (a) Edge-view SEM image of the composite cathode. (b−d) SEM images of the composite cathode under different magnifications. Precipitation of Li_2S is visible within the hollow TiO_{2-x} nanospheres. Scale bars are 2 μm.

tolerate the volume change of sulfur during cycles; (2) the TiO_{2-x} is electrochemical stable during the charge/discharge cycles; (3) the crystalline TiO_{2-x} is mechanically strong due to its ceramic nature. Moreover, the decrease in pore size suggests uniform deposition of insoluble Li_2S_2 and Li_2S on the inner shell of the structure (Figure 6d), which is due to the effective blocking of polysulfides from random diffusion into the electrolyte.

CONCLUSION

In summary, we have successfully fabricated the hydrogen reduced TiO_2 inverse opal and demonstrated its dual functionality in applications as Li−S battery to achieve long cycle life and high capacity. In this rational design, polysulfides are effectively contained in a closed 3D matrix of reduced TiO_2 due to both physical trapping and surface chemical adsorption. The reduced TiO_2 has high electrical conductivity. The small dimension of the nanopores leads to a high specific surface area and thus a high utilization of active material. The hollow structure offers enough space to accommodate the volume change and relax strain during cycling. Therefore, hydrogen reduced TiO_2 inverse opal would have the potential use as a novel electrode structure for Li−S system. And this concept opens up a new avenue for constructing sulfur cathodes with metal oxides.

EXPERIMENTAL METHODS

Synthesis of Hydrogen Reduced Titania and Control Titania. A total of 60 μL of the PS colloidal sphere aqueous suspension (Thermoscientific, 4 w/w %, 780 nm in diameter) was deposited onto an aluminum foil disc (0.025 mm thick, 7/16 in. diameter) by a pipet. The solvent was allowed to evaporate in a fume hood under the air flow rate of 90 sccm for 3 h. The conformal TiO_2 layer was formed at 70 °C using the Cambridge Nanotech Savannah with DI water and titanium tetrachloride ($TiCl_4$) as precursors. The pulse times were 15 and 65 ms, respectively. A total of 600 cycles were performed to create a 30 nm thick TiO_2 thin film. Hydrogen treatment of TiO_2 was performed by a thermal annealing process. The as-prepared TiO_2 coated PS (on Al substrate) was placed into a ceramic combustion boat and heated up to 500 °C in a tube furnace. The ultrapure hydrogen was introduced to the tube under a flow rate of 100 sccm continuously, and the inner pressure was kept at 80 Torr. The temperature was increased from 25 °C at an increasing rate of 5 °C/min and held at 500 °C for 2 h. Afterward, the sample was cooled down to room temperature naturally. The control titania was prepared by heating the TiO_2 coated PS in the box furnace (Thermo Electron Corporation, Lindberg/Blue M) from 25 to 500 °C in air. The heating rate was 5 °C/min, and the sample was held at 500 °C for 2 h.

Synthesis of TiO_{2-x}/Sulfur Composite. Typically, 1 mg of the reduced titania (on an aluminum foil disc with 7/16 in. diameter) was loaded inside a small quartz tube, together with 100 μL of 1% sulfur solution in toluene. The mixture was then dried on a hot plate for 20 min before it was sealed using Teflon tape and baked in a box furnace under argon atmosphere. The baking procedure requires 155 °C with a heating rate of 4.5 °C/min at which sulfur exhibits lowest viscosity. The sample was kept for 12 h at 155 °C before it was washed with methanol for 30 s.

Electrochemical Measurement. The TiO_{2-x}/sulfur composite casted on aluminum foil disc (7/16 in. diameter) was directly utilized as working electrode. The 2032-type coin cells (MTI) were constructed in argon-filled glovebox (MB-200B, Mbraun) with lithium foil as counter/reference electrode. No binder or extra conductive additives were employed. Lithium bis-(trifluoromethanesulfonyl)imide (LiTFSI, 1 M) in cosolvent of 1,3-dioxolane and 1,2-dimethoxyethane (volume ratio 1:1) with lithium nitrite (1 wt %) was used as electrolyte. The weight percentage of sulfur in electrode materials is ~45%. Cyclic voltammetry was performed on an electrochemical station (VMP3, Bio-logic). Galvanostatic cycling was conducted using a 96-channel battery tester (Arbin Instruments). To conduct the Current−voltage measurement, TiO_2 inverse opal thin film (7/16 in. diameter, 15 μm thick) was sandwiched between two aluminum foils connecting to the electrochemical station (VMP3, Bio-logic). The scan rate was 100 mV/s, and the voltage range was from −2 to 2 V.

Characterization. SEM characterization was carried out by using an FEI XL30 Sirion scanning electron microscope with a field emission gun (FEG) source. TEM characterization was carried out by using an FEI Tecnai G2 F20 X-TWIN transmission electron microscope (TEM). The composition and phase of samples was probed *via* X-ray diffraction (XRD, X'Pert Pro, PANalaytcal) with Cu Kα radiation. The electronic environment of samples was investigated through X-ray photoelectron spectroscopy (XPS, Phi5000 VersaProbe, Ulvac-Phi) with Al Kα radiation. Lithiated electrodes after cycling were taken out of the coin cell inside an argon-filled glovebox and washed with acetonitrile (ACN) to extract residual electrolyte and salts. After a drying period of 3 h, the sample was ready for further examination.

Conflict of Interest: The authors declare no competing financial interest.

Acknowledgment. Y.C. acknowledges the support from the Assistant Secretary for Energy Efficiency and Renewable Energy, Office of Vehicle Technologies of the U.S. Department of Energy.

Supporting Information Available: Additional top view and cross sectional SEM images of reduced TiO_2, comparison of cycling performances for reduced TiO_2 and control TiO_2, Current−voltage characteristics of reduced TiO_2 and control TiO_2. This material is available free of charge *via* the Internet at http://pubs.acs.org.

REFERENCES AND NOTES

1. Jacobson, M. Z. Review of Solutions to Global Warming, Air Pollution, and Energy Security. *Energy Environ. Sci.* **2009**, *2*, 148–173.
2. Tarascon, J. M.; Armand, M. Issues and Challenges Facing Rechargeable Lithium Batteries. *Nature* **2001**, *414*, 359–367.
3. Chan, C. K.; Peng, H.; Liu, G.; McIlwrath, K.; Zhang, X. F.; Huggins, R. A.; Cui, Y. High-Performance Lithium Battery Anodes Using Silicon Nanowires. *Nat. Nanotechnol.* **2008**, *3*, 31–35.
4. Cui, L. F.; Ruffo, R.; Chan, C. K.; Peng, H.; Cui, Y. Crystalline-Amorphous Core-Shell Silicon Nanowires for High Capacity and High Current Battery Electrodes. *Nano Lett.* **2008**, *9*, 491–495.
5. Cui, L. F.; Yang, Y.; Hsu, C. M.; Cui, Y. Carbon-Silicon Core-Shell Nanowires as High Capacity Electrode for Lithium Ion Batteries. *Nano Lett.* **2009**, *9*, 3370–3374.
6. Park, M. H.; Kim, M. G.; Joo, J.; Kim, K.; Kim, J.; Ahn, S.; Cui, Y.; Cho, J. Silicon Nanotube Battery Anodes. *Nano Lett.* **2009**, *9*, 3844–3847.
7. Wu, H.; Chan, G.; Choi, J. W.; Ryu, I.; Yao, Y.; McDowell, M. T.; Lee, S. W.; Jackson, A.; Yang, Y.; Hu, L.; *et al.* Stable Cycling

of Double-Walled Silicon Nanotube Battery Anodes through Solid-Electrolyte Interphase Control. *Nat. Nanotechnol.* **2012**, *7*, 310–315.
8. Manthiram, A. Materials Challenges and Opportunities of Lithium Ion Batteries. *J. Phys. Chem. Lett.* **2011**, *2*, 176–184.
9. Ji, X.; Lee, K. T.; Nazar, L. F. A Highly Ordered Nanostructured Carbon-Sulphur Cathode for Lithium-Sulphur Batteries. *Nat. Mater.* **2009**, *8*, 500–506.
10. Shim, J.; Striebel, K. A.; Cairns, E. J. The Lithium/Sulfur Rechargeable Cell: Effects of Electrode Composition and Solvent on Cell Performance. *J. Electrochem. Soc.* **2002**, *149*, A1321–A1325.
11. Mikhaylik, Y. V.; Akridge, J. R. Polysulfide Shuttle Study in the Li/S Battery System. *J. Electrochem. Soc.* **2004**, *151*, A1969–A1976.
12. Ji, X.; Nazar, L. F. Advances in Li-S batteries. *J. Mater. Chem.* **2010**, *20*, 9821–9826.
13. Moon, S.; Jung, Y. H.; Jung, W. K.; Jung, D. S.; Choi, J. W.; Kim, D. K. Encapsulated Monoclinic Sulfur for Stable Cycling of Li-S Rechargeable Batteries. *Adv. Mater.* **2013**, *25*, 6547–6553.
14. Liang, C.; Dudney, N. J.; Howe, J. Y. Hierarchically Structured Sulfur/Carbon Nanocomposite Material for High-Energy Lithium Battery. *Chem. Mater.* **2009**, *21*, 4724–4730.
15. Wu, F.; Chen, J.; Chen, R.; Wu, S.; Li, L.; Chen, S.; Zhao, T. Sulfur/Polythiophene with a Core/Shell Structure: Synthesis and Electrochemical Properties of the Cathode for Rechargeable Lithium Batteries. *J. Phys. Chem. C* **2011**, *115*, 6057–6063.
16. Suo, L.; Hu, Y. S.; Li, H.; Armand, M.; Chen, L. A New Class of Solvent-in-Salt Electrolyte for High-Energy Rechargeable Metallic Lithium Batteries. *Nat. Commun.* **2013**, *4*, 1481.
17. Yamin, H.; Gorenshtein, A.; Penciner, J.; Sternberg, Y.; Peled, E. Lithium Sulfur Battery: Oxidation/Reduction Mechanisms of Polysulfides in THF Solutions. *J. Electrochem. Soc.* **1988**, *135*, 1045–1048.
18. Barchasz, C.; Leprêtre, J. C.; Alloin, F.; Patoux, S. New Insights into the Limiting Parameters of the Li/S Rechargeable Cell. *J. Power Sources.* **2012**, *199*, 322–330.
19. Yang, Y.; Zheng, G.; Cui, Y. Nanostructured Sulfur Cathodes. *Chem. Soc. Rev.* **2013**, *42*, 3018–3032.
20. Zheng, W.; Liu, Y. W.; Hu, X. G.; Zhang, C. F. Novel Nanosized Adsorbing Sulfur Composite Cathode Materials for the Advanced Secondary Lithium Batteries. *Electrochim. Acta* **2006**, *51*, 1330–1335.
21. Zheng, G.; Yang, Y.; Cha, J. J.; Hong, S. S.; Cui, Y. Hollow Carbon Nanofiber-Encapsulated Sulfur Cathodes for High Specific Capacity Rechargeable Lithium Batteries. *Nano Lett.* **2011**, *11*, 4462–4467.
22. Wang, H.; Yang, Y.; Liang, Y.; Robinson, J. T.; Li, Y.; Jackson, A.; Cui, Y.; Dai, H. Graphene-Wrapped Sulfur Particles as a Rechargeable Lithium-Sulfur Battery Cathode Material with High Capacity and Cycling Stability. *Nano Lett.* **2011**, *11*, 2644–2647.
23. Yang, Y.; Yu, G.; Cha, J. J.; Wu, H.; Vosgueritchian, M.; Yao, Y.; Bao, Z.; Cui, Y. Improving the Performance of Lithium-Sulfur Batteries by Conductive Polymer Coating. *ACS Nano* **2011**, *5*, 9187–9193.
24. Xiao, L.; Cao, Y.; Xiao, J.; Schwenzer, B.; Engelhard, M. H.; Saraf, L. V.; Nie, Z.; Exarhos, G. J.; Liu, J. A Soft Approach to Encapsulate Sulfur: Polyaniline Nanotubes for Lithium-Sulfur Batteries with Long Cycle Life. *Adv. Mater.* **2012**, *24*, 1176–1181.
25. Li, W.; Zheng, G.; Yang, Y.; Seh, Z. W.; Liu, N.; Cui, Y. High-Performance Hollow Sulfur Nanostructured Battery Cathode through a Scalable, Room Temperature, One-Step, Bottom-Up Approach. *Proc. Natl. Acad. Sci. U.S.A.* **2013**, *110*, 7148–7153.
26. Seh, Z. W.; Li, W.; Cha, J. J.; Zheng, G.; Yang, Y.; McDowell, M. T.; Hsu, P. C.; Cui, Y. Sulphur-TiO_2 Yolk-Shell Nanoarchitecture with Internal Void Space for Long-Cycle Lithium-Sulphur Batteries. *Nat. Commun.* **2013**, *4*, 1331.
27. Dong, K.; Wang, S.; Zhang, H.; Wu, J. Preparation and Electrochemical Performance of Sulfur-Alumina Cathode Material for Lithium-Sulfur Batteries. *Mater. Res. Bull.* **2013**, *48*, 2079–2083.
28. Sun, F.; Wang, J.; Long, D.; Qiao, W.; Ling, L.; Lv, C.; Cai, R. A High-Rate Lithium-Sulfur Battery Assisted by Nitrogen-Enriched Mesoporous Carbons Decorated with Ultrafine La_2O_3 Nanoparticles. *J. Mater. Chem. A* **2013**, *1*, 13283–13289.
29. Zhang, Y.; Wu, X.; Feng, H.; Wang, L.; Zhang, A.; Xia, T.; Dong, H. Effect of Nanosized $Mg_{0.8}Cu_{0.2}O$ on Electrochemical Properties of Li/S Rechargeable Batteries. *Int. J. Hydrogen Energy* **2009**, *34*, 1556–1559.
30. Zhang, Y.; Zhao, Y.; Yermukhambetova, A.; Bakenov, Z.; Chen, P. Ternary Sulfur/Polyacrylonitrile/$Mg_{0.6}Ni_{0.4}O$ Composite Cathodes for High Performance Lithium/Sulfur Batteries. *J. Mater. Chem. A* **2013**, *1*, 295–301.
31. Evers, S.; Yim, T.; Nazar, L. F. Understanding the Nature of Absorption/Adsorption in Nanoporous Polysulfide Sorbents for the Li-S Battery. *J. Phys. Chem. C* **2012**, *116*, 19653–19658.
32. Orilall, M. C.; Abrams, N. M.; Lee, J.; DiSalvo, F. J.; Wiesner, U. Highly Crystalline Inverse Opal Transition Metal Oxides *via* a Combined Assembly of Soft and Hard Chemistries. *J. Am. Chem. Soc.* **2008**, *130*, 8882–8883.
33. Kim, O. H.; Cho, Y. H.; Kang, S. H.; Park, H. Y.; Kim, M.; Lim, J. W.; Chung, D. Y.; Lee, M. J.; Choe, H.; Sung, Y. E. Ordered Macroporous Platinum Electrode and Enhanced Mass Transfer in Fuel Cells Using Inverse Opal Structure. *Nat. Commun.* **2013**, *4*, 2473.
34. Ye, X.; Qi, L. Two-Dimensionally Patterned Nanostructures Based on Monolayer Colloidal Crystals: Controllable Fabrication, Assembly, and Applications. *Nano Today* **2011**, *6*, 608–631.
35. Zhang, X.; Xie, Y. Recent Advances in Free-Standing Two-Dimensional Crystals with Atomic Thickness: Design, Assembly and Transfer Strategies. *Chem. Soc. Rev.* **2013**, *42*, 8187–8199.
36. Wang, G.; Wang, H.; Ling, Y.; Tang, Y.; Yang, X.; Fitzmorris, R. C.; Wang, C.; Zhang, J. Z.; Li, Y. Hydrogen-Treated TiO_2 Nanowire Arrays for Photoelectrochemical Water Splitting. *Nano Lett.* **2011**, *11*, 3026–3033.
37. Zhang, J. T.; Chao, X.; Asher, S. A. Asymmetric Free-Standing 2-D Photonic Crystal Films and Their Janus Particles. *J. Am. Chem. Soc.* **2013**, *135*, 11397–11401.
38. Shin, J. Y.; Joo, J. H.; Samuelis, D.; Maier, J. Oxygen-Deficient $TiO_{2-\delta}$ Nanoparticles *via* Hydrogen Reduction for High Rate Capability Lithium Batteries. *Chem. Mater.* **2011**, *24*, 543–551.
39. Lu, X.; Wang, G.; Zhai, T.; Yu, M.; Gan, J.; Tong, Y.; Li, Y. Hydrogenated TiO_2 Nanotube Arrays for Supercapacitors. *Nano Lett.* **2012**, *12*, 1690–1696.
40. Stefik, M.; Heiligtag, F. J.; Niederberger, M.; Grätzel, M. Improved Nonaqueous Synthesis of TiO_2 for Dye-Sensitized Solar Cells. *ACS Nano* **2013**, *7*, 8981–8989.
41. Xia, T.; Zhang, C.; Oyler, N. A.; Chen, X. Hydrogenated TiO_2 Nanocrystals: A Novel Microwave Absorbing Material. *Adv. Mater.* **2013**, *25*, 6905–6910.
42. Chen, X.; Liu, L.; Yu, P. Y.; Mao, S. S. Increasing Solar Absorption for Photocatalysis with Black Hydrogenated Titanium Dioxide Nanocrystals. *Science* **2011**, *331*, 746–750.
43. Hebenstreit, E. L. D.; Hebenstreit, W.; Diebold, U. Adsorption of Sulfur on TiO_2 (110) Studied with STM, LEED and XPS: Temperature-Dependent Change of Adsorption Site Combined with O-S Exchange. *Surf. Sci.* **2000**, *461*, 87–97.
44. Mayer, J. T.; Diebold, U.; Madey, T. E.; Garfunkel, E. Titanium and Reduced Titania Overlayers on Titanium Dioxide (110). *J. Electron Spectrosc. Relat. Phenom.* **1995**, *73*, 1–11.
45. Yan, G.; Zhang, M.; Hou, J.; Yang, J. Photoelectrochemical and Photocatalytic Properties of N+S Co-Doped TiO_2 Nanotube Array Films under Visible Light Irradiation. *Mater. Chem. Phys.* **2011**, *129*, 553–557.
46. Chen, X.; Glans, P. A.; Qiu, X.; Dayal, S.; Jennings, W. D.; Smith, K. E.; Burda, C.; Guo, J. X-ray Spectroscopic Study of the Electronic Structure of Visible-Light Responsive N-, C- and S-Doped TiO_2. *J. Electron Spectrosc. Relat. Phenom.* **2008**, *162*, 67–73.

47. Martinez, H.; Auriel, C.; Gonbeau, D.; Loudet, M.; Pfister-Guillouzo, G. Studies of 1T TiS_2 by STM, AFM and XPS: The Mechanism of Hydrolysis in Air. *Appl. Surf. Sci.* **1996**, *93*, 231–235.
48. Yuan, L.; Yuan, H.; Qiu, X.; Chen, L.; Zhu, W. Improvement of Cycle Property of Sulfur-Coated Multi-Walled Carbon Nanotubes Composite Cathode for Lithium/Sulfur Batteries. *J. Power Sources.* **2009**, *189*, 1141–1146.
49. Li, N.; Liu, G.; Zhen, C.; Li, F.; Zhang, L.; Cheng, H. M. Battery Performance and Photocatalytic Activity of Mesoporous Anatase TiO_2 Nanospheres/Graphene Composites by Template-Free Self-Assembly. *Adv. Funct. Mater.* **2011**, *21*, 1717–1722.
50. Wang, Z.; Lou, X. W. TiO_2 Nanocages: Fast Synthesis, Interior Functionalization and Improved Lithium Storage Properties. *Adv. Mater.* **2012**, *24*, 4124–4129.
51. Pfanzelt, M.; Kubiak, P.; Wohlfahrt-Mehrens, M. Nanosized TiO_2 Rutile with High Capacity and Excellent Rate Capability. *Electrochem. Solid-State Lett.* **2010**, *13*, A91–A94.
52. Reddy, M. A.; Kishore, M. S.; Pralong, V.; Varadaraju, U. V.; Raveau, B. Lithium Intercalation into Nanocrystalline Brookite TiO_2. *Electrochem. Solid-State Lett.* **2007**, *10*, A29–A31.
53. Yao, H.; Zheng, G.; Li, W.; McDowell, M. T.; Seh, Z.; Liu, N.; Lu, Z.; Cui, Y. Crab Shells as Sustainable Templates from Nature for Nanostructured Battery Electrodes. *Nano Lett.* **2013**, *13*, 3385–3390.
54. Lide, D. R., Ed. *CRC Handbook of Chemistry and Physics*, 94th ed. [Online]; CRC Press: Boca Raton, FL, 2013; p 84.